# Supplementary information

## Experimental details

Samples with nominal composition $Ba_{10}(PO_4)_6(Co_xOH_{1-2x})_2$, $x$ = 0.05 (**1**), 0.3 (**2**, **2a**), and 0.5 (**3**) were prepared as follows. Stoichiometric quantities of $BaCO_3$, $(NH_4)_2HPO_4$, and $Co_3O_4$ with 2% excess of $BaCO_3$ were grinded and mixed in an agate mortar (of a total mass of 5 g approx.). The powder was heated to 400 °C for 0.5 h, annealed at this temperature for 0.5 h, heated to 600°C for 0.5 h, annealed at this temperature for 0.5 h, heated to 800°C for 0.5 h, annealed at this temperature for 2.5 h. The furnace cooled powder was grinded and annealed at 1150°C for 4 h. The precursor was grinded, pressed in pellets, annealed at 1300°C for 4 h, and air quenched. The last procedure was repeated once more. The resulting pellets were annealed at 1400°C or 1450°C for 1 – 2 hours and air quenched. All procedures were performed in air atmosphere.

Synchrotron powder X-ray diffraction was carried out at the Diamond Light Source, I12-JEEP beamline[1] ($\lambda$ = 0.23369 Å) using 2D area flat panel detector Pixium RF4343. Wavelength calibration and data reduction was performed using the software DAWN.[2,3] High-precision powder X-ray diffraction was conducted using a D8 Bruker-AXS powder diffractometer (Cu-Kα1 radiation from a primary Ge(111) Johansson-type monochromator; Lynx-Eye position-sensitive detector with an opening angle of 3.5°) in Bragg-Brentano geometry in the $2\theta$ range 10 – 120°, step 0.009°. The crystal structures were refined with the JANA 2006 computer program.[4]

Scanning electron microscopy with energy-dispersive X-ray (EDX) analysis was performed on a Supra 50 VP LEO electron microscope.

Magnetic properties were measured on a Quantum Design SQUID VSM (**I**) and on a Quantum Design SQUID MPMS (**II**) in the temperature range 1.8 – 300 K and magnetic field range -70 – +70 kOe. A piece of a ceramic sample (50 - 200 mg) was fixed with GE-varnish (< 0.3 mg) on a quartz rod (**I**) or deposited into a gelatin capsule in a plastic straw (**II**). dc-magnetization was measured in a dc-SQUID mode. Magnetization decay was registered for 2 hour. ac susceptibility ($\chi_{ac}$) was measured under an ac field of 2.5 – 3 Oe in the frequency range 0.1 – 945 Hz (**I**) or 0.1 – 1420 Hz (**II**) and in the temperature range 1.8 – 50 K. The data were corrected for the diamagnetism of a gelatin capsule if necessary. The core diamagnetism was subtracted from the magnetization using Pascal's constants. The generalized Debye model was applied to fit simultaneously the $\chi'$ and $\chi''$ components of $\chi_{ac}(\omega)$ ($\omega = 2\pi f$) using the following equations[5]

$$\chi'(\omega) = \chi_s + \frac{(\chi_0 - \chi_s)\left[1 + (\omega\tau)^{1-\alpha}\sin 1/2\alpha\pi\right]}{1 + 2(\omega\tau)^{1-\alpha}\sin 1/2\alpha\pi + (\omega\tau)^{2(1-\alpha)}},$$

$$\chi''(\omega) = \frac{(\chi_0 - \chi_s)(\omega\tau)^{1-\alpha}\cos 1/2\alpha\pi}{1 + 2(\omega\tau)^{1-\alpha}\sin 1/2\alpha\pi + (\omega\tau)^{2(1-\alpha)}}.$$

Relaxation time $\tau$, low- and high-frequency susceptibilities $\chi_0$ and $\chi_s$, their difference $\Delta\chi = F$ (as a contribution of slow-relaxing magnetization), and a relaxation time distribution parameter $\alpha$ were estimated. All the parameters were refined simultaneously for the temperature interval 15 – 35 K, for which a $\chi''(\omega)$ local maximum is observed. Then $\Delta\chi(T)$ was fitted by Curie-Weiss equation. In order to escape correlations, for higher temperatures, $\Delta\chi$ was fixed to the value calculated using the Curie-Weiss parameters, while all other parameters were refined.

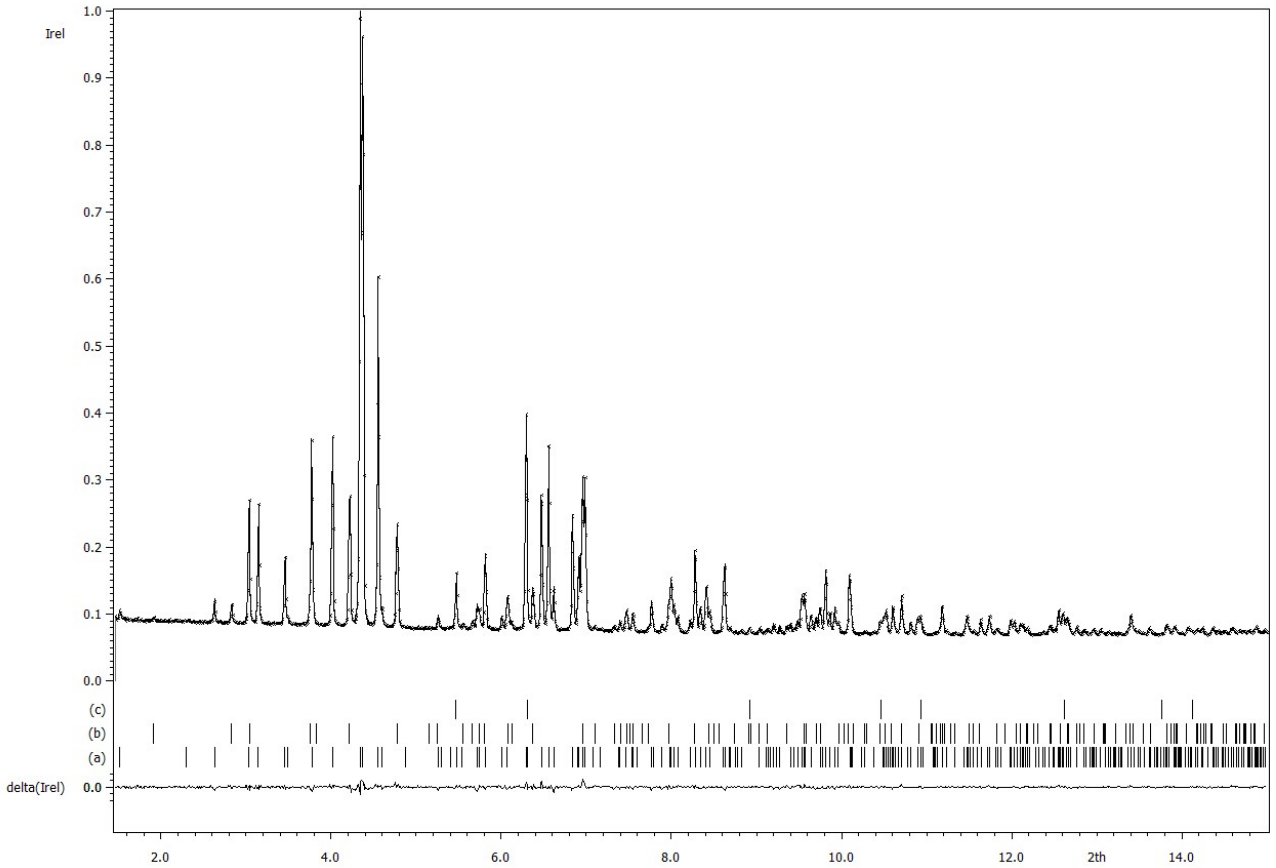


Figure S1. Synchrotron powder X-ray diffraction pattern of **3**. Observed (crosses), calculated (solid line) and difference (solid line below) plots. Positions of Bragg reflections are shown as strokes underneath: (a) the main apatite-type phase $Ba_{10}(PO_4)_6(Co_{0.33}O_{0.72}H_y)_2$, (b) $Ba_3(PO_4)_2$ (12.8%), and (c) CoO (1.4%).

Table S1. Crystal structure refinement data for $Ba_{10}(PO_4)_6(Co_{0.33}O_{0.72}H_y)_2$ (sample **3**).

| | |
|---|---|
| Temperature (K) | 293 K |
| Wavelength (Å) | 0.23369 |
| Space group | $P6_3/m$ |
| $a$ (Å) | 10.1926(1) |
| $c$ (Å) | 7.7532(1) |
| $V$ (Å$^3$) | 697.56(2) |
| $Z$ | 1 |
| $2\theta$ range (deg.) | 1.47 - 15 |
| $R_{wp}$ | 0.014 |
| $R_{all}$ | 0.023 |
| $\Delta F_{max}$, $\Delta F_{min}$ (e Å$^{-3}$) | 0.66, -0.63 |

Table S2. Atomic parameters and thermal displacement parameters (Å$^2$) for $Ba_{10}(PO_4)_6(Co_{0.33}O_{0.72}H_y)_2$ (sample **3**).

| Atom | Ba(1) | Ba(2) | P | O(1)[a)] | O(2) | O(3) | O(4) | Co[b)] |
|---|---|---|---|---|---|---|---|---|
| Site | 4f | 6h | 6h | 6h | 6h | 12i | 4e | 12i |
| SOF | 1 | 1 | 1 | 1 | 1 | 1 | 0.36(2) | 0.055(2) |
| *x* | 1/3 | 0.24375(17) | 0.3996(6) | 0.3440(14) | 0.5560(14) | 0.3537(7) | 0 | 0.033(6) |
| *y* | 2/3 | 0.98102(18) | 0.3626(7) | 0.4748(13) | 0.4441(13) | 0.2732(8) | 0 | 0 |
| *z* | -0.0006(4) | 1/4 | 1/4 | 1/4 | 1/4 | 0.0894(8) | 0.204(5) | 0 |
| $U_{eq}$, $U_{iso}$ | 0.0261(5) | 0.0208(10) | 0.016(2) | 0.028(2) | 0.028(2) | 0.028(2) | 0.028(2) | 0.07(2) |
| $U_{11}$ | 0.0266(7) | 0.0330(14) | | | | | | |
| $U_{22}$ | 0.0266(7) | 0.0222(12) | | | | | | |
| $U_{33}$ | 0.0250(10) | 0.0321(9) | | | | | | |
| $U_{12}$ | 0.0133(3) | 0.0101(13) | | | | | | |
| $U_{13}$ | 0 | 0 | | | | | | |
| $U_{23}$ | 0 | 0 | | | | | | |

[a)]An overal $U_{iso}$ value for all oxygen atoms was refined.

[b)]Initially obtained large $U_{11}$ and $U_{22}$ of 0.15 for Co atom in comparison with $U_{33}$ = 0.03 suggested the Co atom to disorder mostly in *ab*-plain. As it was not possible to get a proper displacement direction due to strong correlations, *y* and *z* of the Co atom were fixed to zero values.

Table S3. Selected interatomic distances (Å) and angles (degrees) in the crystal structure of $Ba_{10}(PO_4)_6(Co_{0.33}O_{0.72}H_y)_2$ (sample **3**).

| | | | | | |
|---|---|---|---|---|---|
| Ba(1)-O(1) | 2.797(11) | 3x | Co-O(4) | 1.62(5) | |
| Ba(1)-O(2) | 2.759(12) | 3x | Co-O(3) | 3.03(6) | |
| Ba(1)-O(3) | 3.011(8) | 3x | O(1)-P-O(2) | 107.6(9) | |
| Ba(2)-O(1) | 2.913(4) | | O(1)-P-O(3) | 110.2(5) | 2x |
| Ba(2)-O(2) | 2.768(9) | | O(2)-P-O(3) | 106.6(5) | 2x |
| Ba(2)-O(3) | 2.756(4) | 2x | O(3)-P-O(3) | 115.3(6) | |
| Ba(2)-O(3) | 2.888(4) | 2x | O(4)-Co-O(4) | 156(4) | |
| Ba(2)-O(4) | 2.611(4) | | | | |
| P-O(1) | 1.509(18) | | | | |
| P-O(2) | 1.380(14) | | | | |
| P-O(3) | 1.474(7) | 2x | | | |

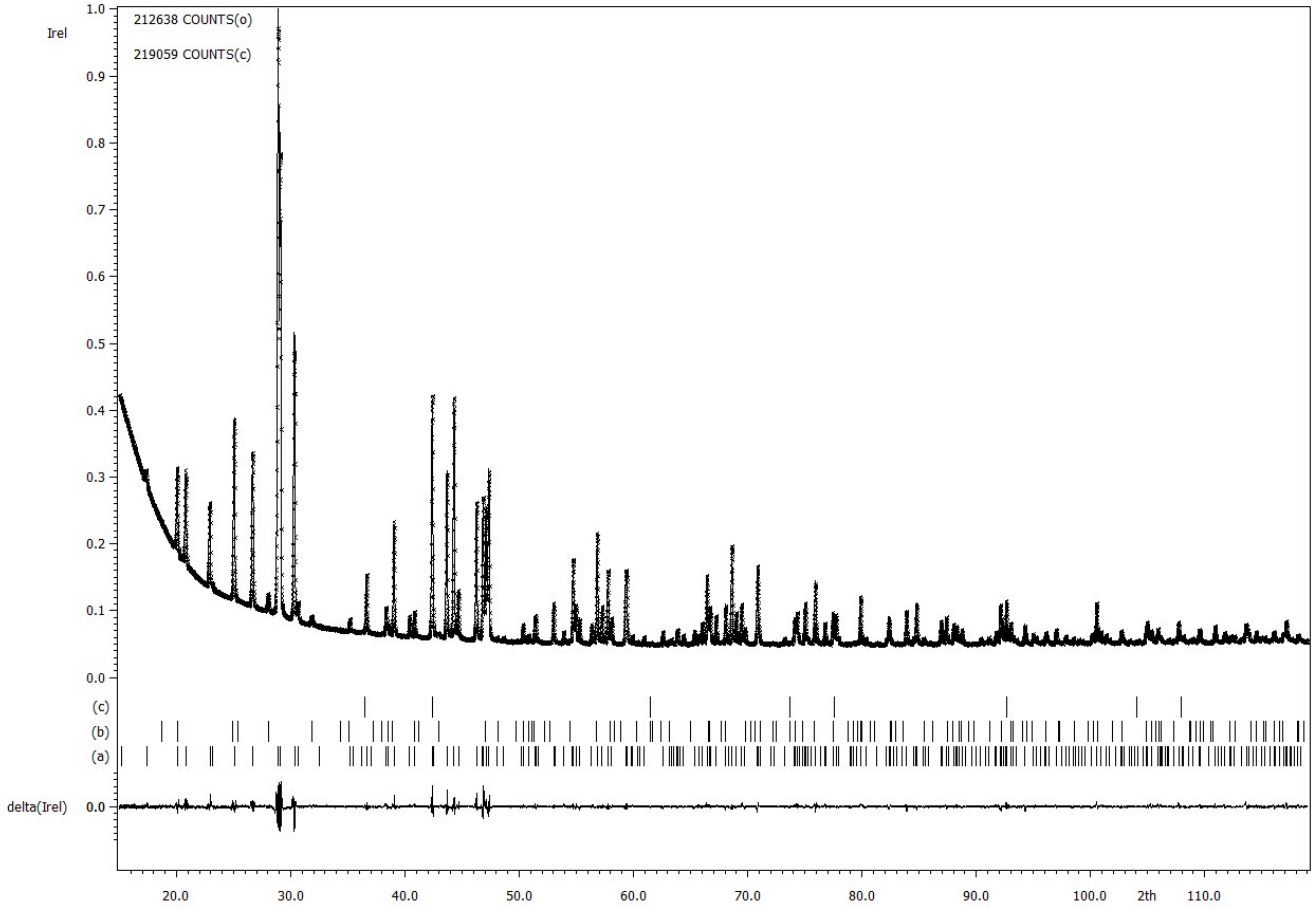


Figure S2. Powder X-ray diffraction pattern of **2**. Observed (crosses), calculated (solid line) and difference (solid line below) plots. Positions of Bragg reflections are shown as strokes underneath: (a) the main apatite-type phase $Ba_{10}(PO_4)_6(Co_{0.23}O_{0.88}H_y)_2$, (b) $Ba_3(PO_4)_2$ (2.18%), and (c) CoO (0.33%). Apatite-type phase lattice: Space group $P6_3/m$, $a$ = 10.1962(2) Å, $c$ = 7.7486(2) Å.

Table S4. Atomic parameters and thermal displacement parameters (Å$^2$) for $Ba_{10}(PO_4)_6(Co_{0.23}O_{0.88}H_y)_2$ (sample **2**). $R_{wp}$ = 0.019 , $R_{all}$ = 0.021.

| Atom | Ba(1) | Ba(2) | P | O(1) | O(2) | O(3) | O(4) | Co |
|---|---|---|---|---|---|---|---|---|
| Site | 4f | 6h | 6h | 6h | 6h | 12i | 4e | 2b |
| SOF | 1 | 1 | 1 | 1 | 1 | 1 | 0.44(3) | 0.228(11) |
| $x$ | 1/3 | 0.24379(15) | 0.4028(6) | 0.3398(13) | 0.5787(13) | 0.3443(8) | 0 | 0 |
| $y$ | 2/3 | 0.98083(15) | 0.3702(6) | 0.4840(12) | 0.4538(12) | 0.2627(10) | 0 | 0 |
| $z$ | -0.0005(3) | 1/4 | 1/4 | 1/4 | 1/4 | 0.0894(7) | 0.199(6) | 0 |
| $U_{eq}$, $U_{iso}$ | 0.0165(8) | 0.0182(10) | 0.015(2) | 0.018(4) | 0.008(3) | 0.025(3) | 0.11(2) | 0.023(9) |
| $U_{11}$ | 0.0178(10) | 0.0225(14) | | | | | | 0.035(12) |
| $U_{22}$ | 0.0178(10) | 0.0089(12) | | | | | | 0.035(12) |
| $U_{33}$ | 0.0139(11) | 0.0201(11) | | | | | | 0.001(13) |
| $U_{12}$ | 0.0089(5) | 0.0056(11) | | | | | | 0.017(6) |
| $U_{13}$ | 0 | 0 | | | | | | 0 |
| $U_{23}$ | 0 | 0 | | | | | | 0 |

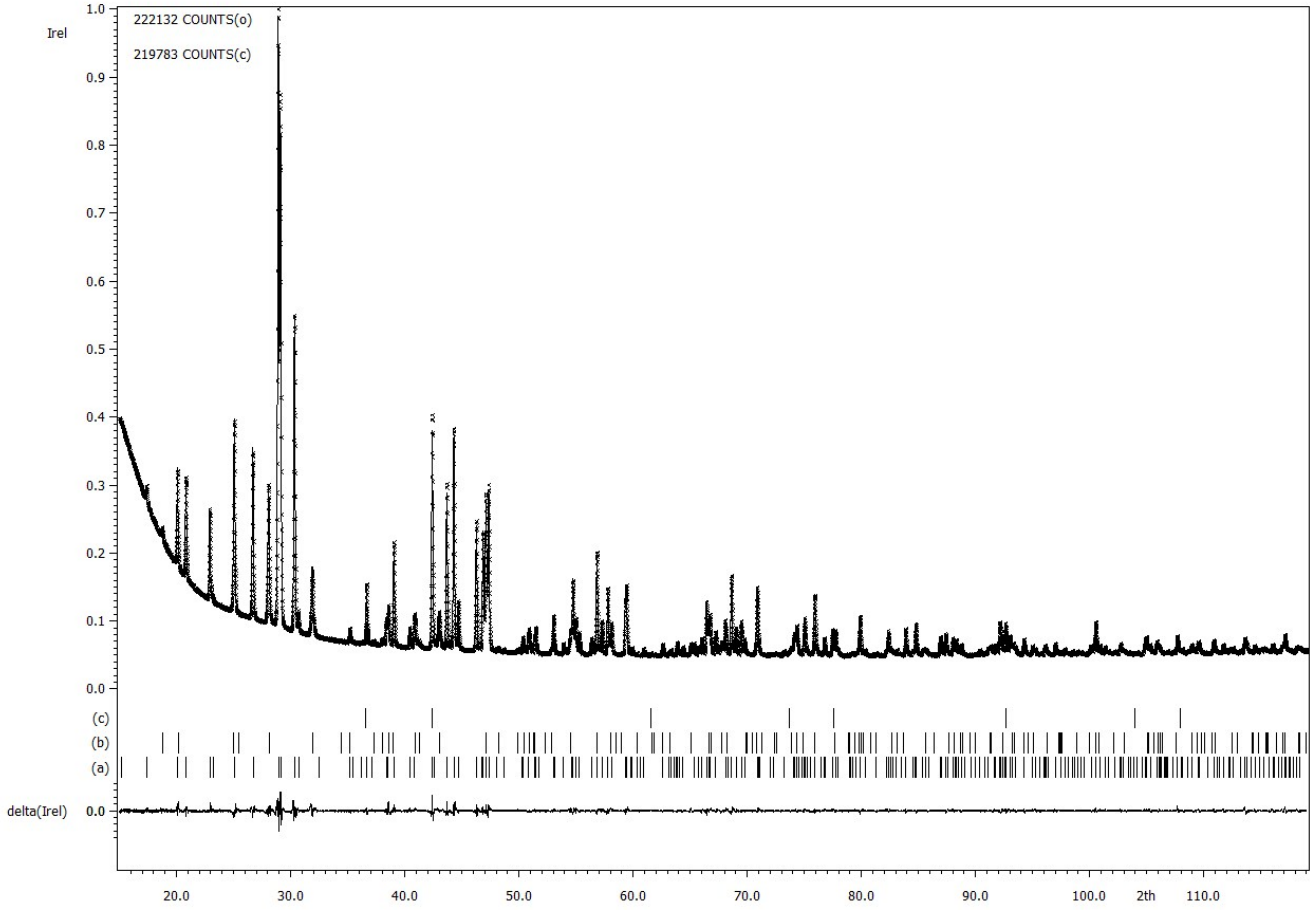


Figure S3. Powder X-ray diffraction pattern of **2a**. Observed (crosses), calculated (solid line) and difference (solid line below) plots. Positions of Bragg reflections are shown as strokes underneath: (a) the main apatite-type phase $Ba_{10}(PO_4)_6(Co_{0.23}O_{0.98}H_y)_2$, (b) $Ba_3(PO_4)_2$ (14.4%), and (c) CoO (0.37%). Apatite-type phase lattice: Space group $P6_3/m$, $a$ = 10.1983(2) Å, $c$ = 7.7508(2) Å.

Table S5. Atomic parameters and thermal displacement parameters (Å$^2$) for $Ba_{10}(PO_4)_6(Co_{0.23}O_{0.98}H_y)_2$ (sample **2a**). $R_{wp}$ = 0.017, $R_{all}$ = 0.014.

| Atom | Ba(1) | Ba(2) | P | O(1) | O(2) | O(3) | O(4) | Co |
|---|---|---|---|---|---|---|---|---|
| Site | 4f | 6h | 6h | 6h | 6h | 12i | 4e | 2b |
| SOF | 1 | 1 | 1 | 1 | 1 | 1 | 0.49(4) | 0.235(17) |
| $x$ | 1/3 | 0.24442(18) | 0.4024(7) | 0.3391(15) | 0.5748(15) | 0.3434(9) | 0 | 0 |
| $y$ | 2/3 | 0.98104(19) | 0.3699(8) | 0.4829(15) | 0.4553(15) | 0.2646(11) | 0 | 0 |
| $z$ | -0.0006(4) | 1/4 | 1/4 | 1/4 | 1/4 | 0.0920(9) | 0.189(7) | 0 |
| $U_{eq}$, $U_{iso}$ | 0.0122(7) | 0.0151(11) | 0.011(2) | 0.013(4) | 0.009(4) | 0.020(3) | 0.11(3) | 0.060(16) |
| $U_{11}$ | 0.0140(9) | 0.0182(14) | | | | | | 0.09(2) |
| $U_{22}$ | 0.0140(9) | 0.0074(13) | | | | | | 0.09(2) |
| $U_{33}$ | 0.0086(10) | 0.0156(11) | | | | | | 0.01(2) |
| $U_{12}$ | 0.0070(5) | 0.0033(13) | | | | | | 0.044(11) |
| $U_{13}$ | 0 | 0 | | | | | | 0 |
| $U_{23}$ | 0 | 0 | | | | | | 0 |

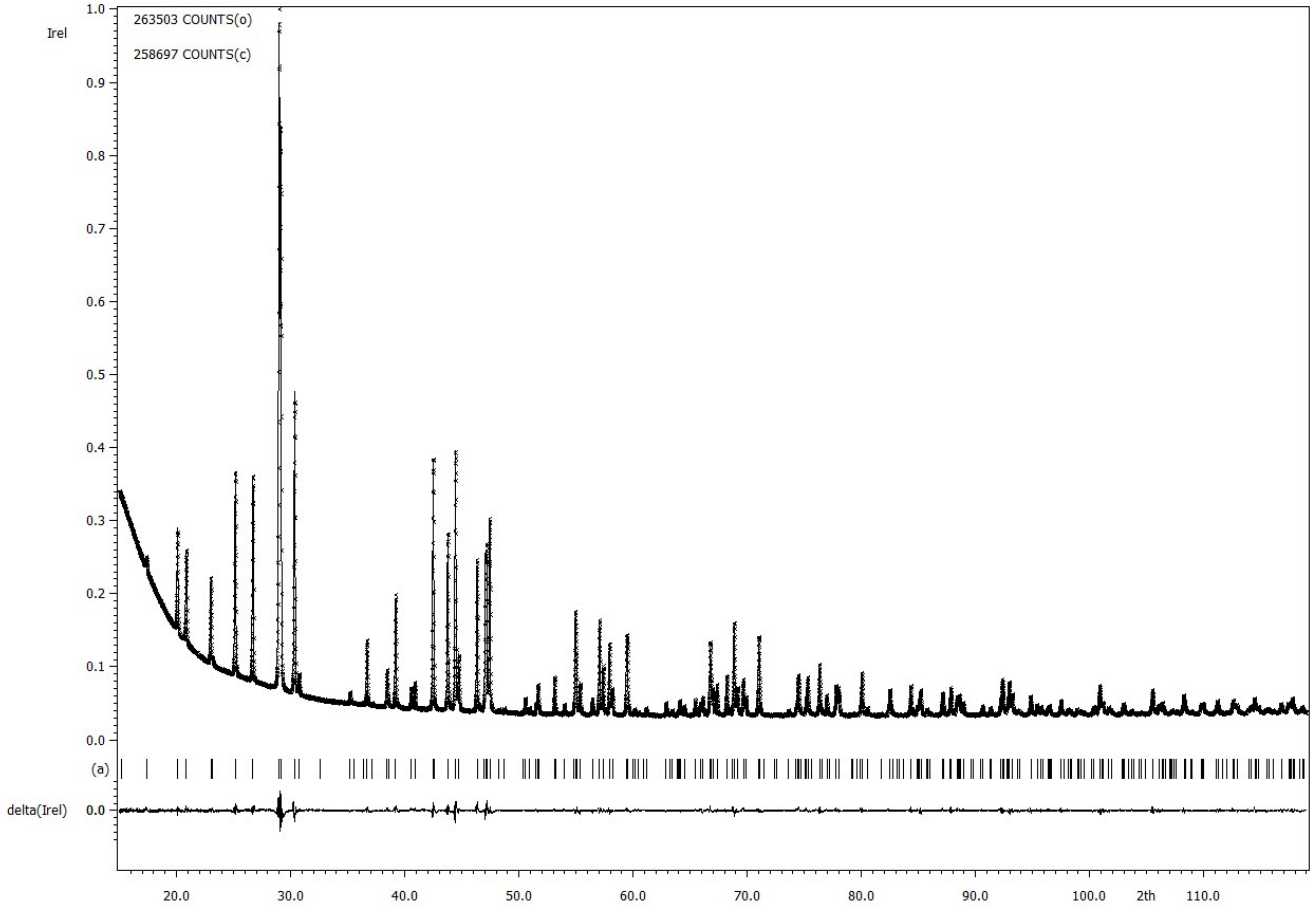


Figure S4. Powder X-ray diffraction pattern of **1**. Observed (crosses), calculated (solid line) and difference (solid line below) plots. Positions of Bragg reflections are shown as strokes underneath: (a) the main apatite-type phase $Ba_{10}(PO_4)_6(Co_{0.05}O_{0.74}H_y)_2$. Apatite-type phase lattice: Space group $P6_3/m$, $a$ = 10.1808(2) Å, $c$ = 7.7106(2) Å.

Table S6. Atomic parameters and thermal displacement parameters (Å$^2$) for $Ba_{10}(PO_4)_6(Co_{0.05}O_{0.74}H_y)_2$ (sample **1**). $R_{wp}$ = 0.020, $R_{all}$ = 0.019.

| Atom | Ba(1) | Ba(2) | P | O(1) | O(2) | O(3) | O(4) | O(5)/Co |
|---|---|---|---|---|---|---|---|---|
| Site | 4f | 6h | 6h | 6h | 6h | 12i | 4e | 2b |
| SOF | 1 | 1 | 1 | 1 | 1 | 1 | 0.236(16) | 0.27(2)/0.05 |
| $x$ | 1/3 | 0.24032(16) | 0.4007(6) | 0.3401(15) | 0.5802(15) | 0.3453(8) | 0 | 0 |
| $y$ | 2/3 | 0.98101(17) | 0.3690(7) | 0.4864(15) | 0.4627(15) | 0.2658(9) | 0 | 0 |
| $z$ | -0.0009(3) | 1/4 | 1/4 | 1/4 | 1/4 | 0.0907(8) | 0.179(5) | 0 |
| $U_{eq}$, $U_{iso}$ | 0.0141(6) | 0.0160(10) | 0.012(2) | 0.027(5) | 0.016(4) | 0.022(3) | 0.02 | 0.02 |
| $U_{11}$ | 0.0141(8) | 0.0198(13) | | | | | | |
| $U_{22}$ | 0.0141(8) | 0.0096(12) | | | | | | |
| $U_{33}$ | 0.0142(9) | 0.0154(9) | | | | | | |
| $U_{12}$ | 0.0071(4) | 0.0049(11) | | | | | | |
| $U_{13}$ | 0 | 0 | | | | | | |
| $U_{23}$ | 0 | 0 | | | | | | |

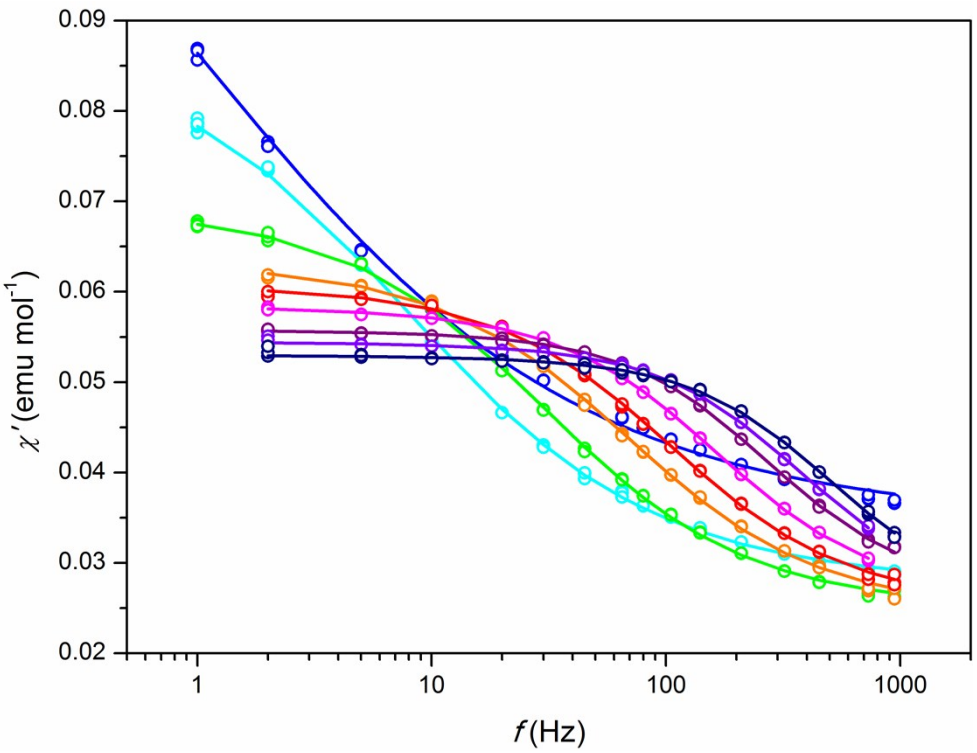
0.09
0.08
0.07
0.06
0.05
0.04
0.03
0.02
χ′(emu mol-1)
1
10
100
1000
f(Hz)

(a)

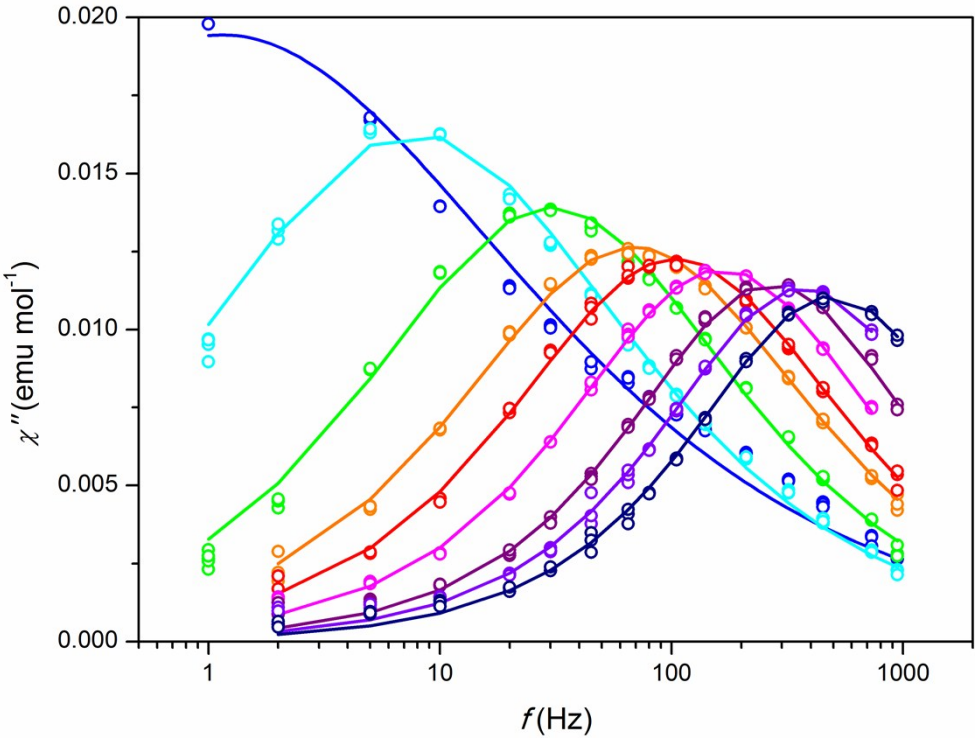
0.020
0.015
0.010
0.005
0.000
χ″(emu mol-1)
1
10
100
1000
f(Hz)

(b)

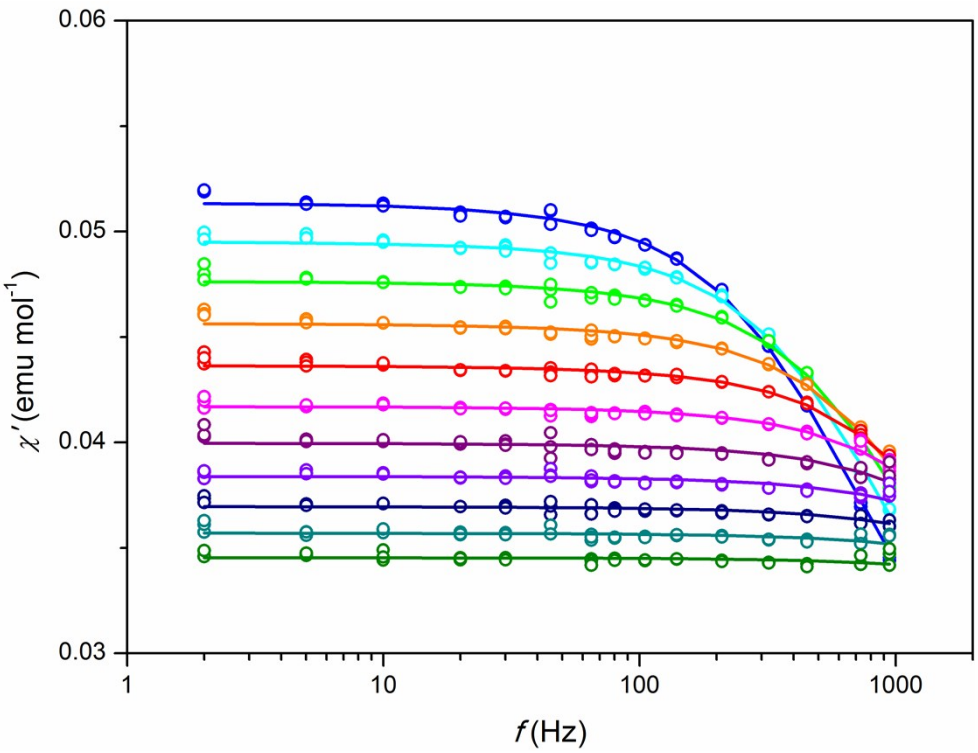


(c)

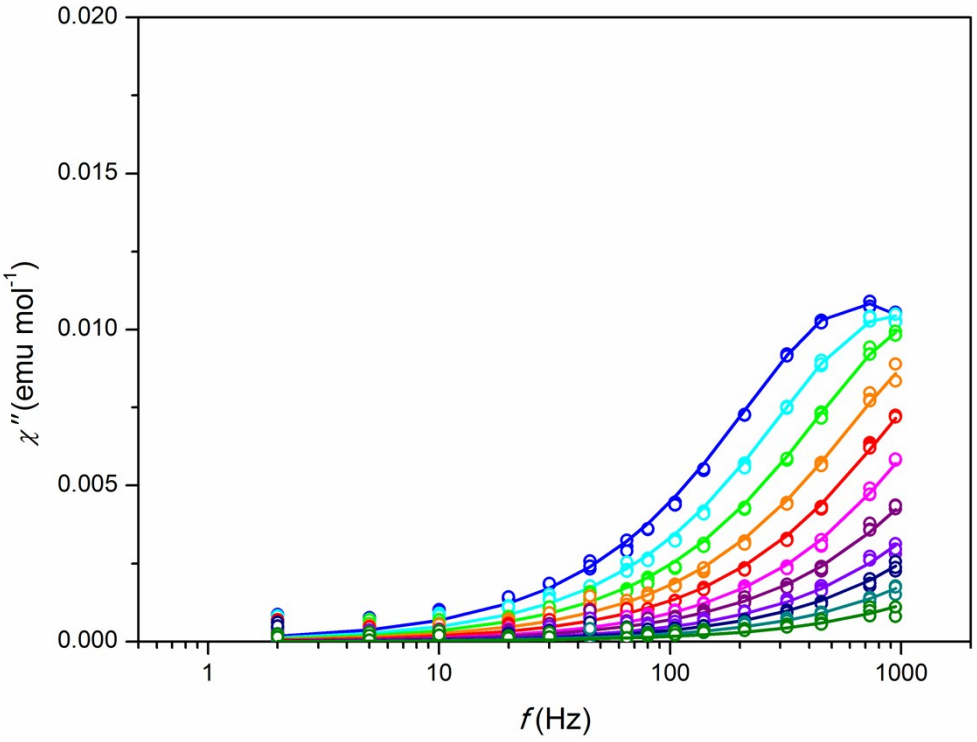


(d)

Figure S5. Frequency (*f*) dependence of ac susceptibility per mol of Co under zero magnetic field for **3**. (a) and (c) – in-phase susceptibility $\chi'$, (b) and (d) – out-of-phase susceptibility $\chi''$. Symbols – experimental points, lines – fitting. The measurement temperature designation: (a) and (b) – blue, cyan, green, orange, red, magenta, purple, violet, navy – 10, 15, 20, 24, 26, 28, 30, 31, 32 K; (c) and (d) - blue, cyan, green, orange, red, magenta, purple, violet, navy, dark cyan, olive – from 33 to 43 K with a step of 1 K.

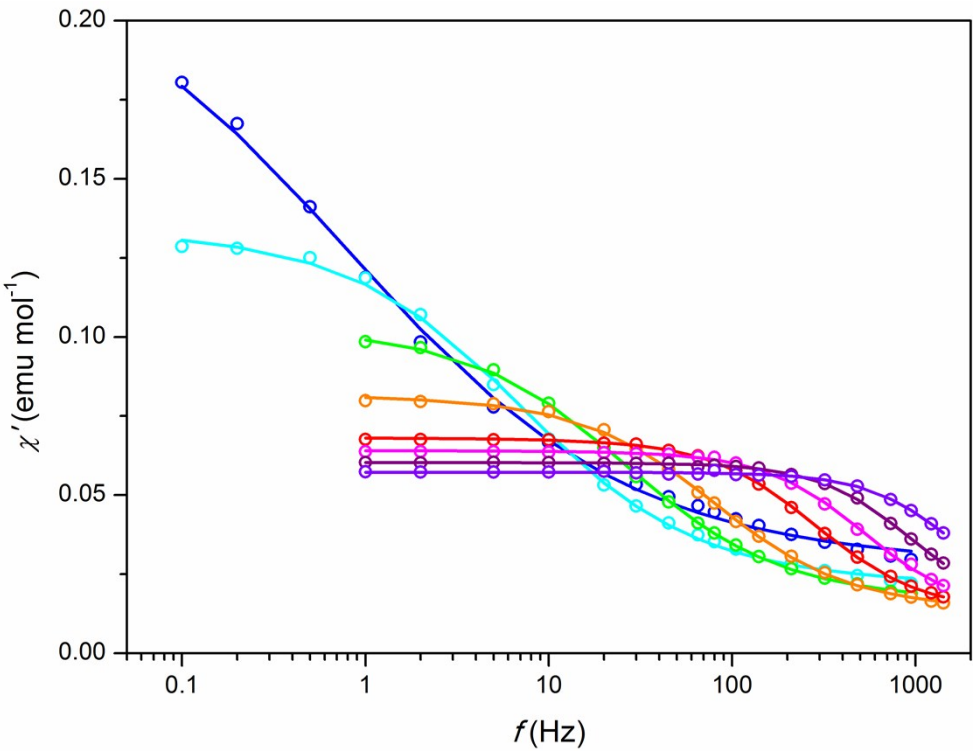
0.20
0.15
0.10
0.05
0.00
χ′(emu mol-1)
0.1
1
10
100
1000
f(Hz)

(a)

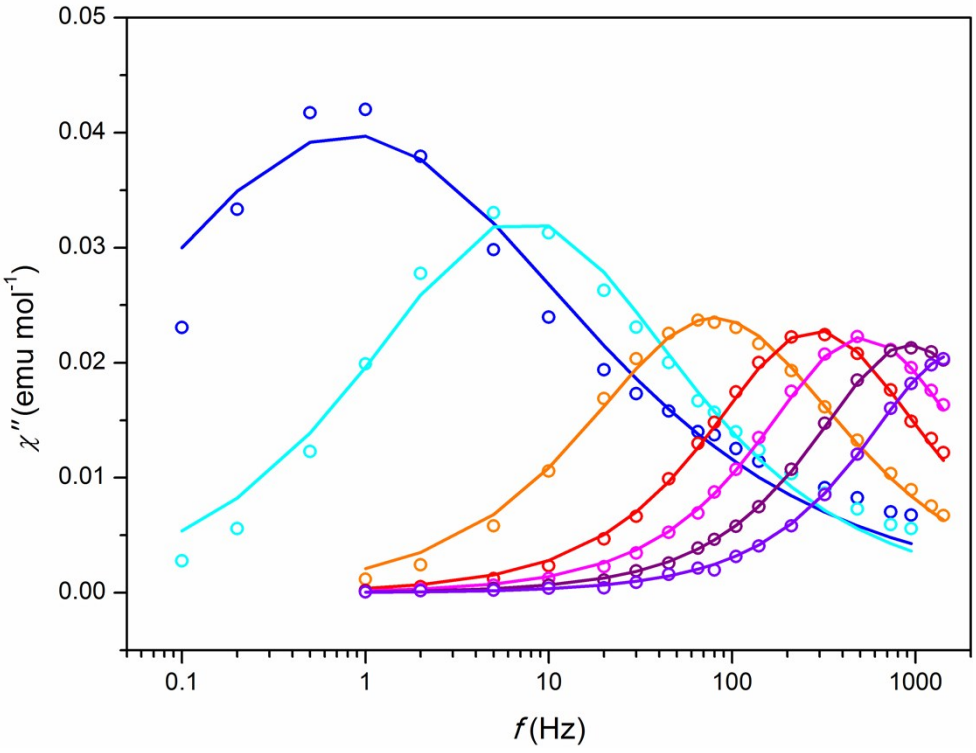
0.05
0.04
0.03
0.02
0.01
0.00
χ″(emu mol-1)
0.1
1
10
100
1000
f(Hz)

(b)

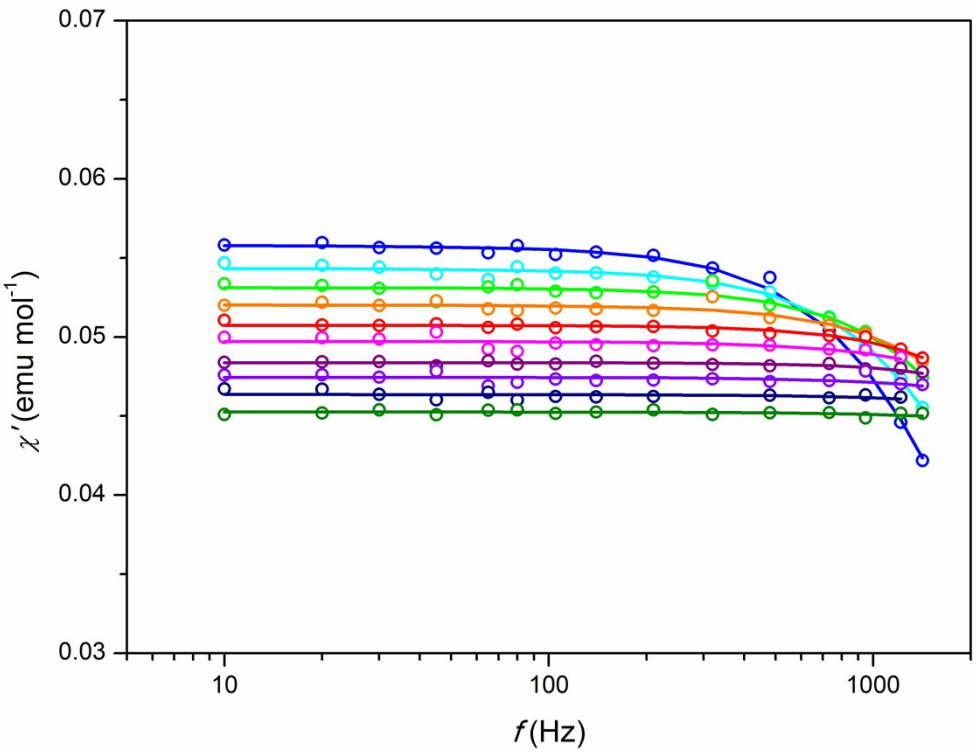


(c)

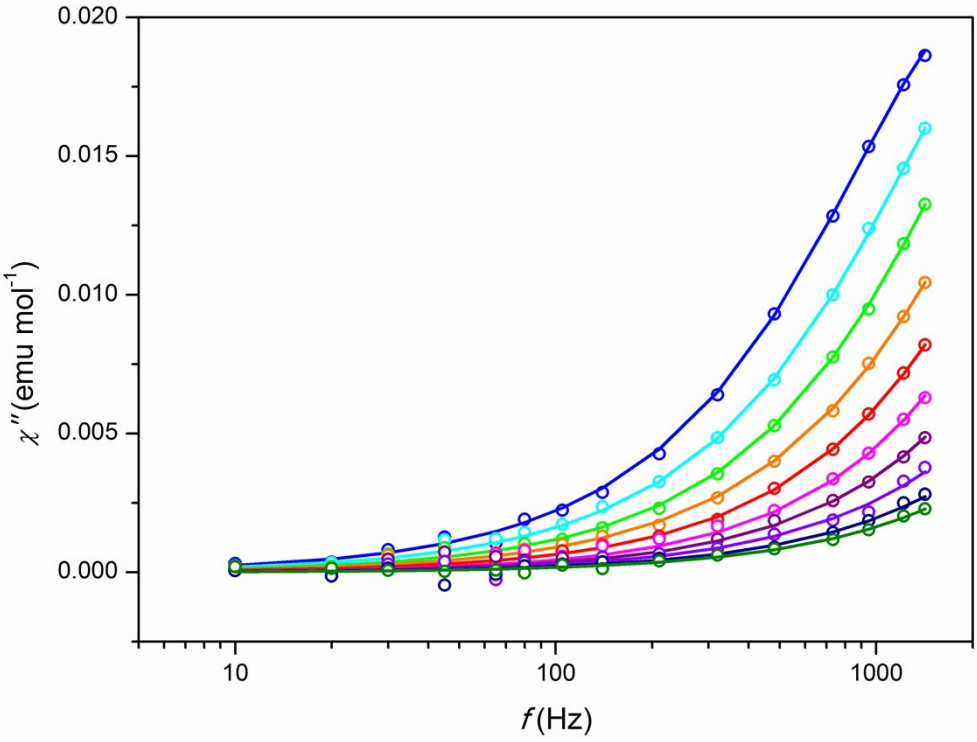


(d)

Figure S6. Frequency (*f*) dependence of ac susceptibility per mol of Co under zero magnetic field for **2**. (a) and (c) – in-phase susceptibility $\chi'$, (b) and (d) – out-of-phase susceptibility $\chi''$. Symbols – experimental points, lines – fitting. The measurement temperature designation: (a) and (b) – blue, cyan, green, orange, red, magenta, purple, violet, – 10, 15, 20, 25, 30, 32, 34, 36; (c) and (d) - blue, cyan, green, orange, red, magenta, purple, violet, navy, olive – from 37 to 46 K with a step of 1 K.

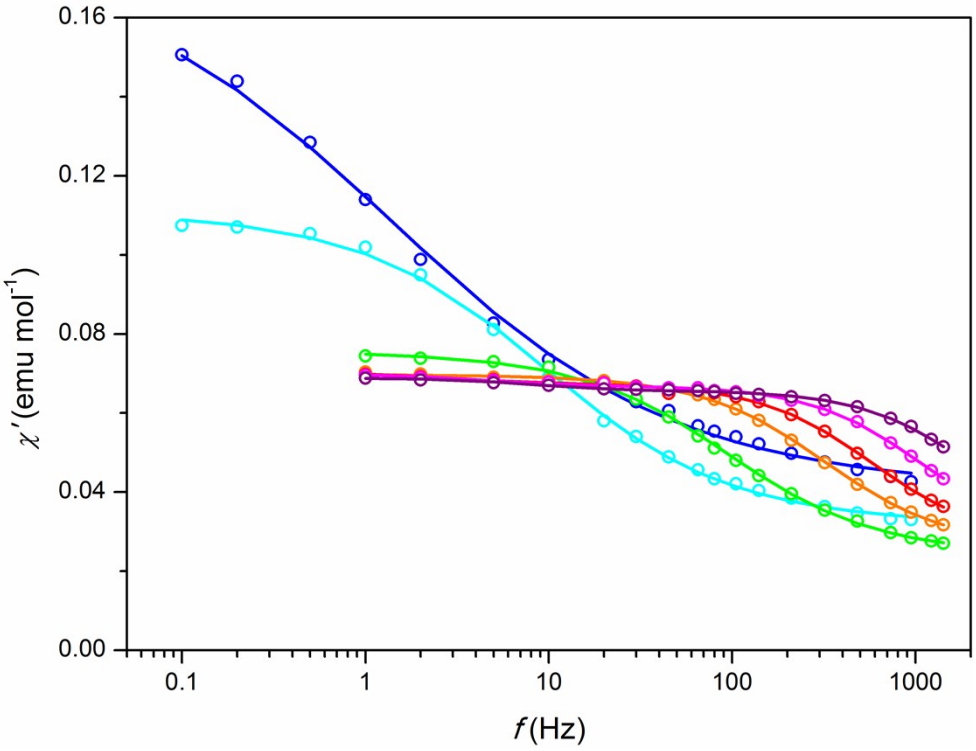
0.16
0.12
0.08
0.04
0.00
χ′(emu mol-1)
0.1
1
10
100
1000
f(Hz)

(a)

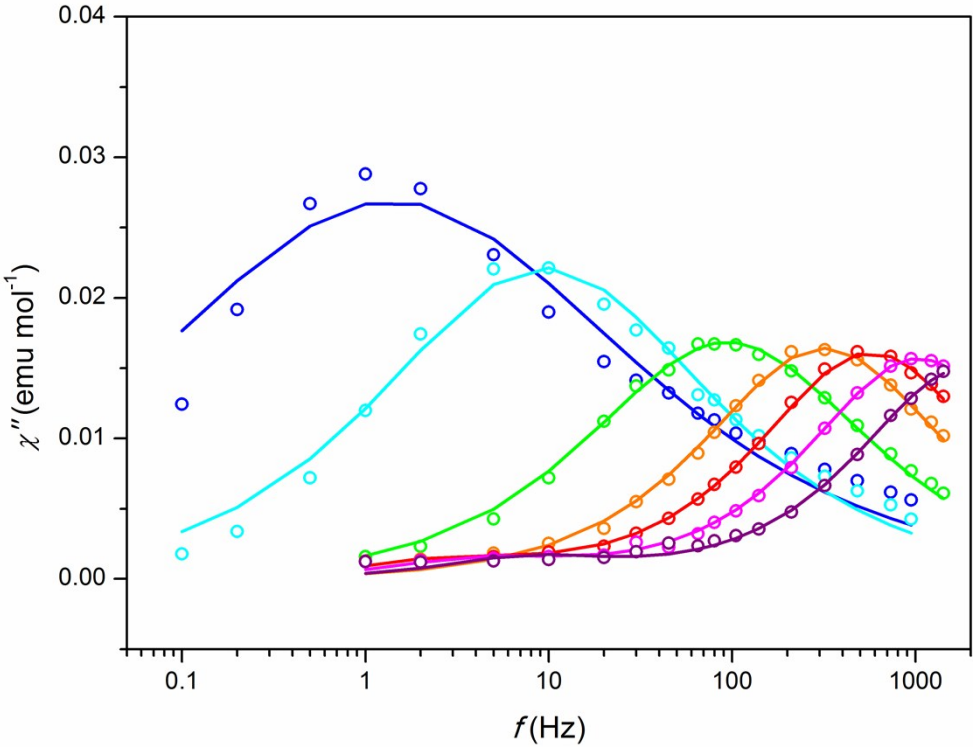
0.04
0.03
0.02
0.01
0.00
χ″(emu mol-1)
0.1
1
10
100
1000
f(Hz)

(b)

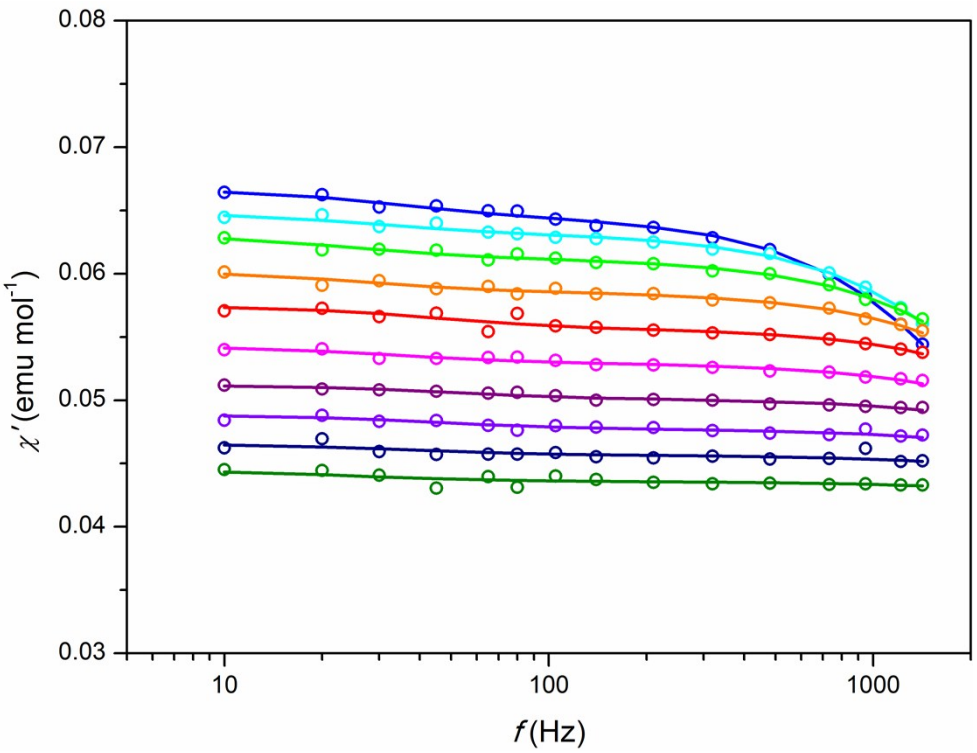


(c)

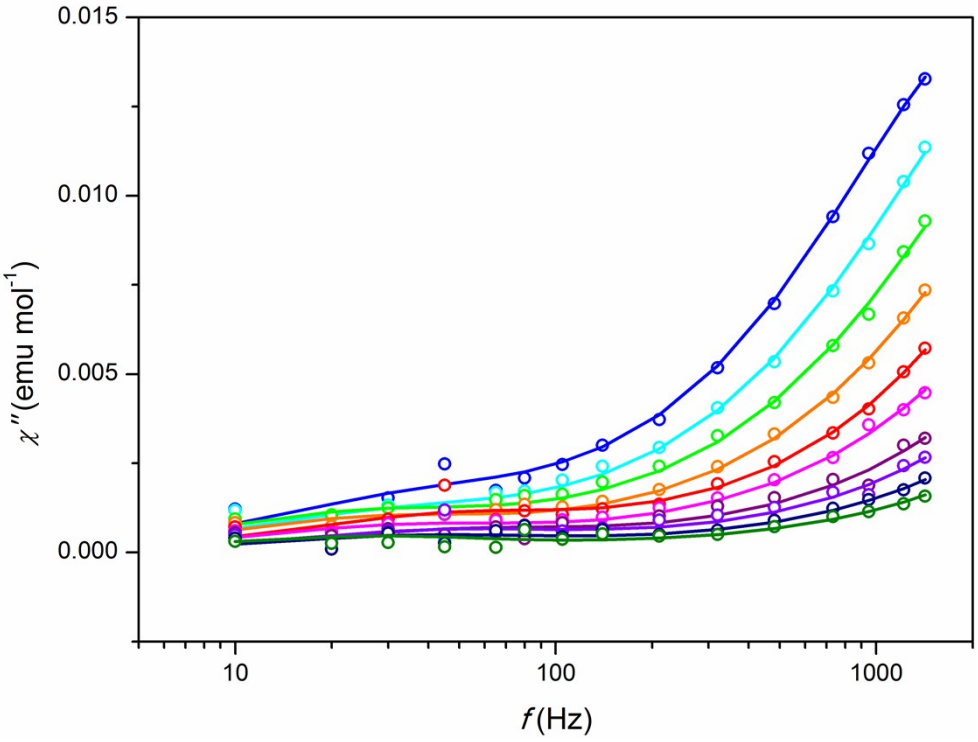


(d)

Figure S7. Frequency (*f*) dependence of ac susceptibility per mol of Co under zero magnetic field for **2a**. (a) and (c) – in-phase susceptibility $\chi'$, (b) and (d) – out-of-phase susceptibility $\chi''$. Symbols – experimental points, lines – fitting. The measurement temperature designation: (a) and (b) – blue, cyan, green, orange, red, magenta, purple, – 10, 15, 25, 30, 32, 34, 36; (c) and (d) - blue, cyan, green, orange, red, magenta, purple, violet, navy, olive – from 37 to 46 K with a step of 1 K. The fitting included a small contribution (a few per cent) of a second relaxation process at a lower frequency.

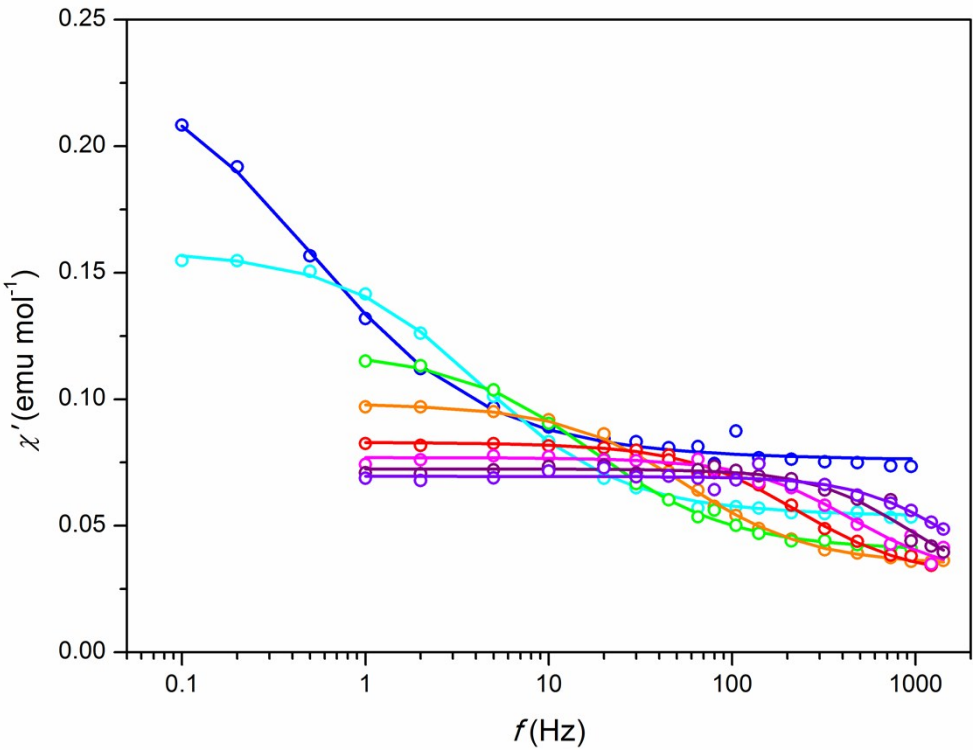
0.25
0.20
0.15
0.10
0.05
0.00
χ′(emu mol-1)
0.1
1
10
100
1000
f(Hz)

(a)

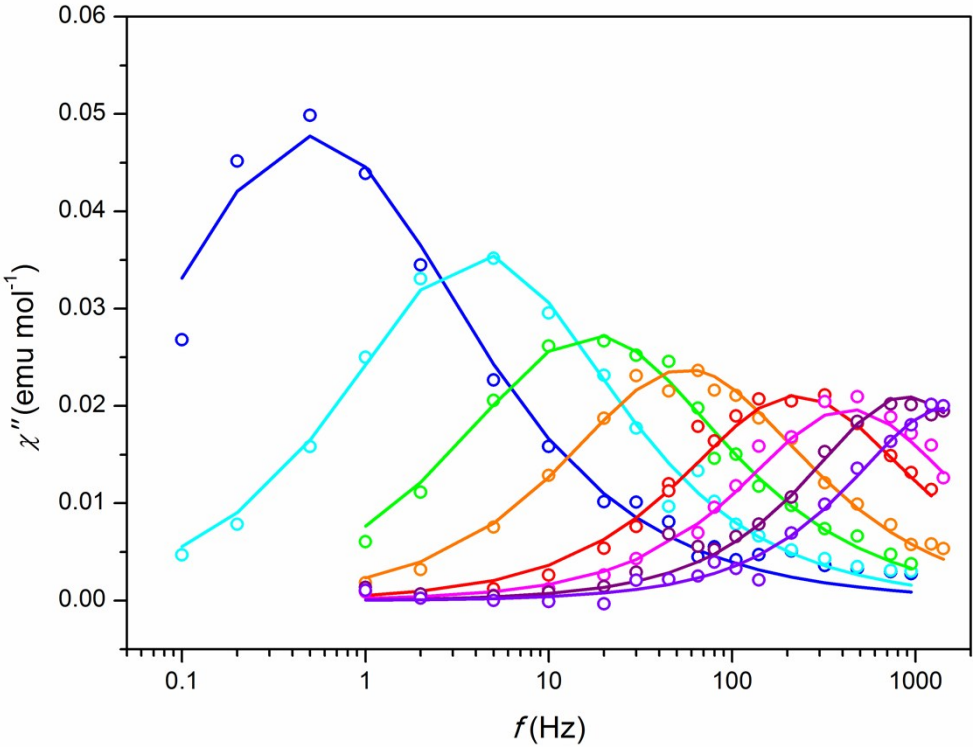
0.06
0.05
0.04
0.03
0.02
0.01
0.00
χ″(emu mol-1)
0.1
1
10
100
1000
f(Hz)

(b)

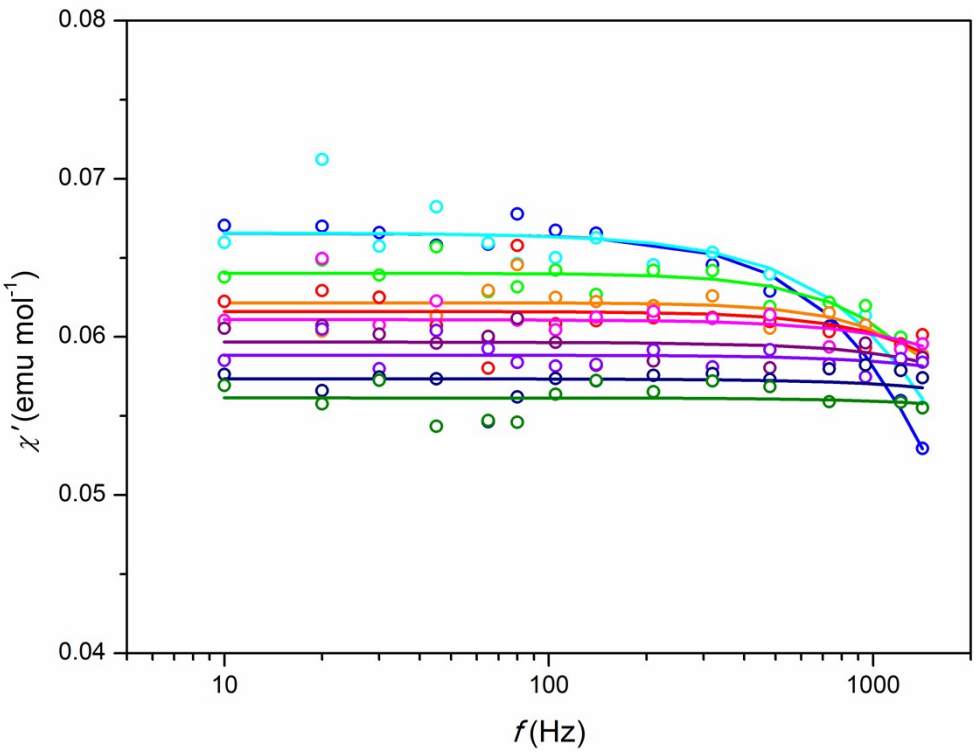


(c)

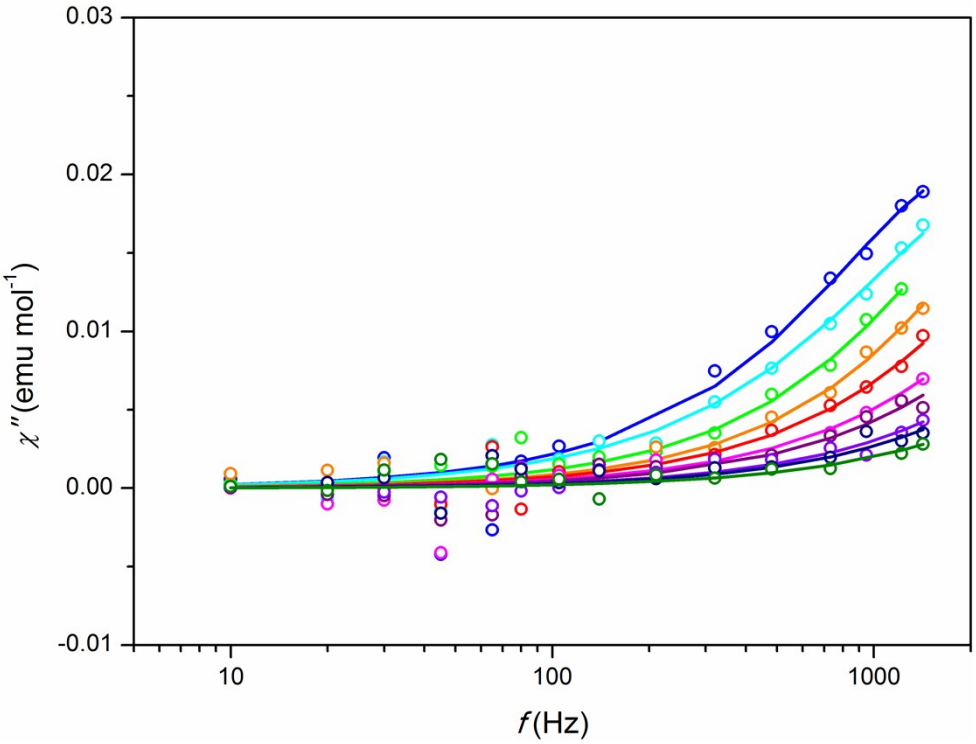


(d)

Figure S8. Frequency (*f*) dependence of ac susceptibility per mol of Co under zero magnetic field for **1**. (a) and (c) – in-phase susceptibility $\chi'$, (b) and (d) – out-of-phase susceptibility $\chi''$. Symbols – experimental points, lines – fitting. The measurement temperature designation: (a) and (b) – blue, cyan, green, orange, red, magenta, purple, violet, – 10, 15, 20, 25, 30, 32, 34, 36; (c) and (d) - blue, cyan, green, orange, red, magenta, purple, violet, navy, olive – from 37 to 46 K with a step of 1 K.

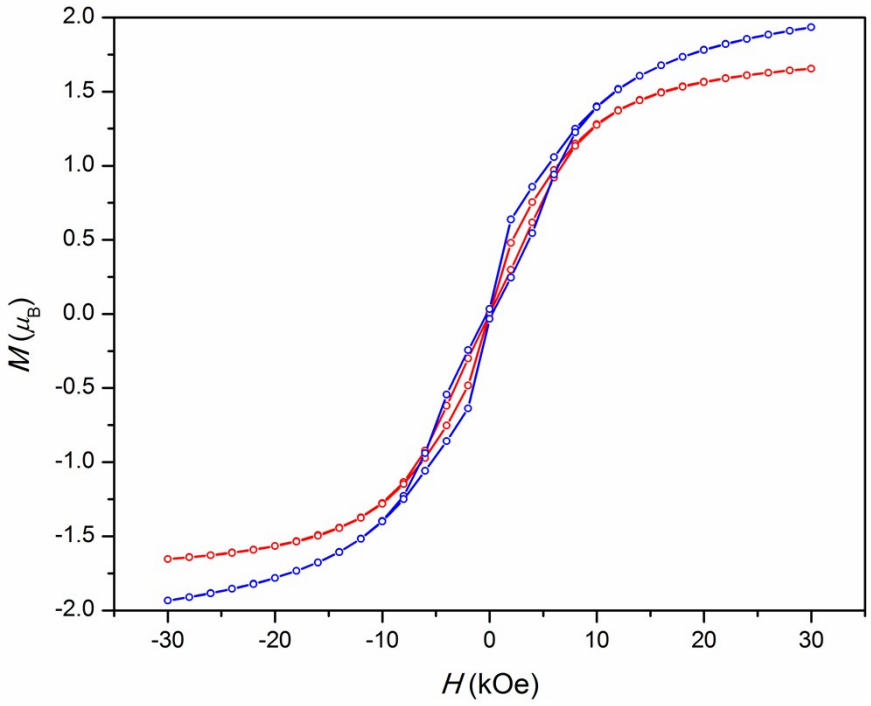


Figure S9. Magnetization $M$ per 1 Co atom vs. magnetic field $H$ at $T$ = 1.8 K measured with a field sweeping rate of ca. 15 Oe $s^{-1}$. Blue symbols – **1**, red symbols – **2**.

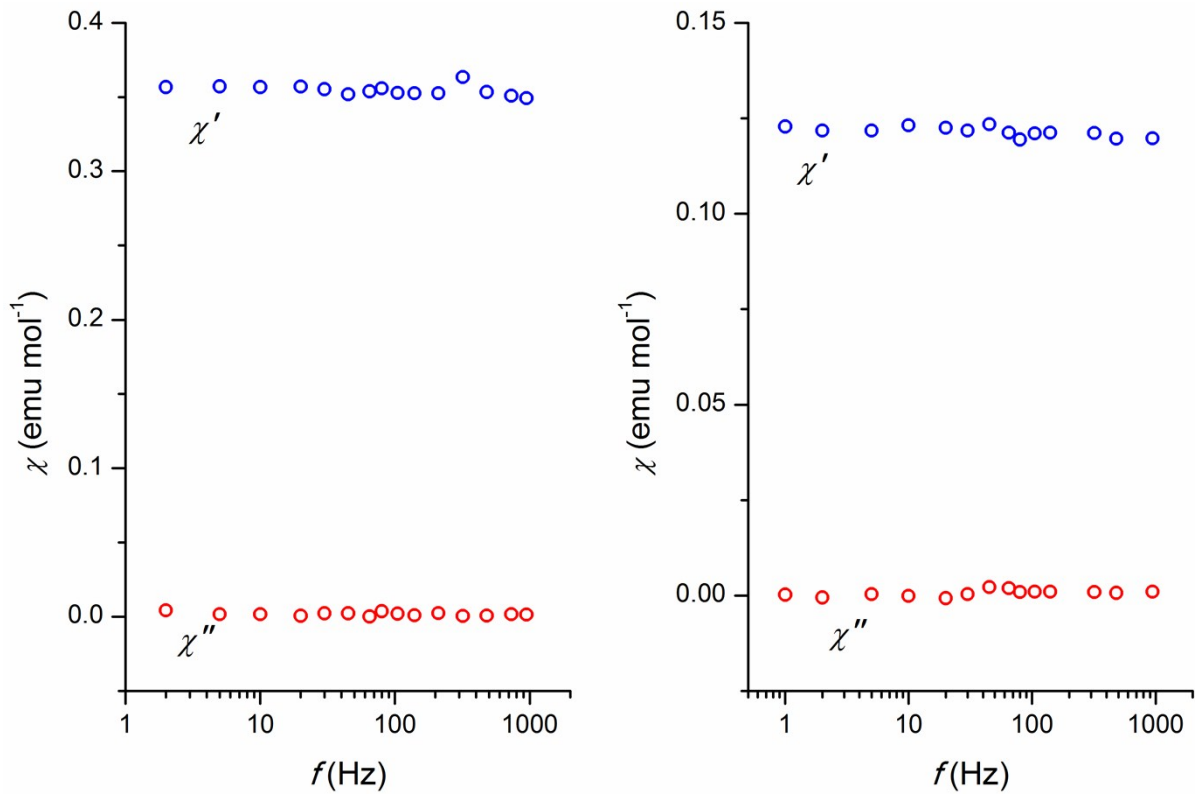


(a) (b)

Figure S10. ac susceptibility of **4**. (a) at 5 K in a dc magnetic field of 4 kOe, (b) at 20 K in zero magnetic field.

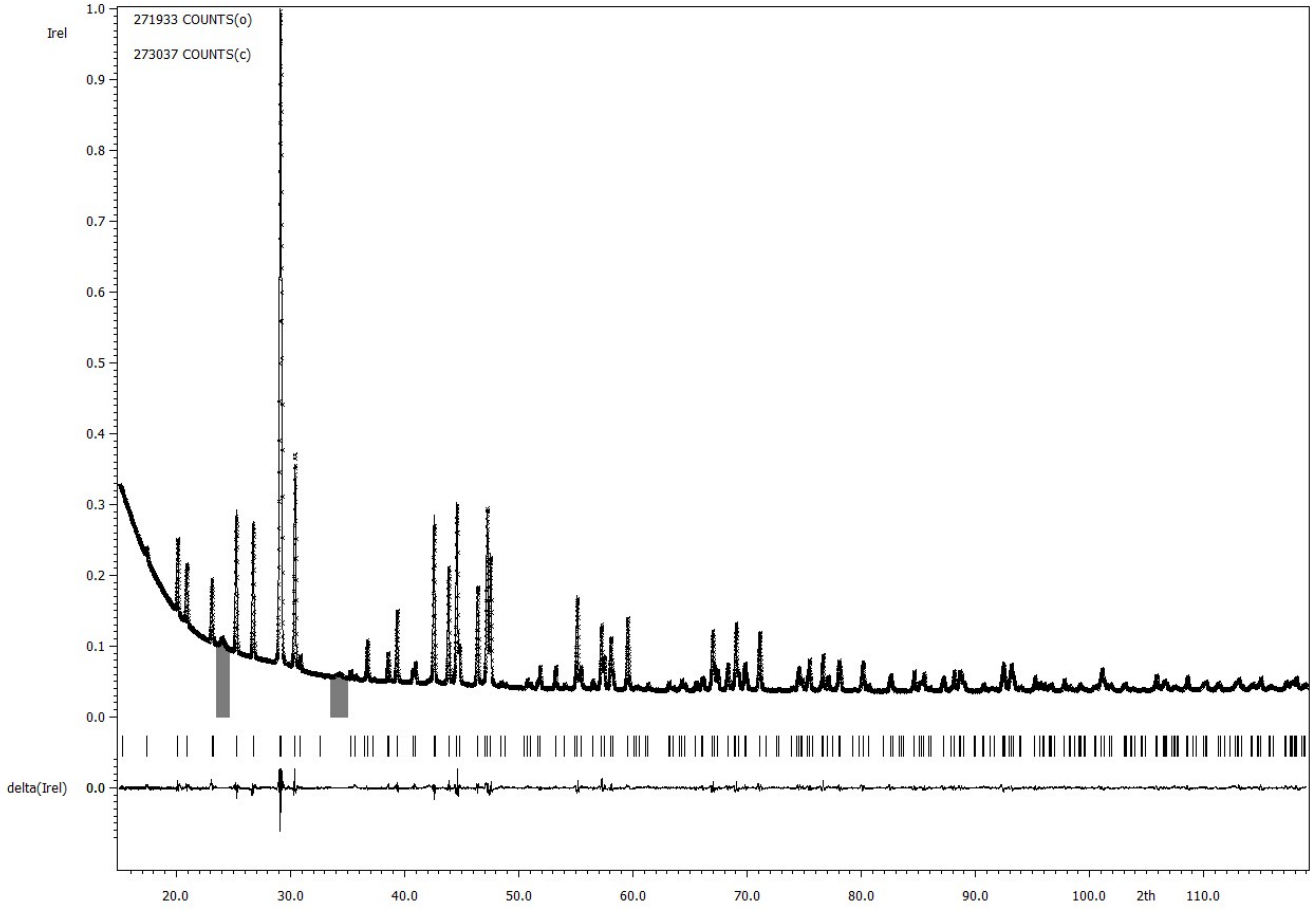


Figure S11. Powder X-ray diffraction pattern of **4**. Observed (crosses), calculated (solid line) and difference (solid line below) plots. Positions of Bragg reflections are shown as strokes underneath. The main apatite-type phase $Ba_{10}(PO_4)_6(OH_y)_2$*0.05$Co_2O_3$, space group $P6_3/m$, $a$ = 10.1772(2) Å, $c$ = 7.6869(2) Å. Two extra peaks with intensity below 1.5% belong to an admixture of $BaCO_3$. The corresponding $2\theta$ intervals have been excluded (shaded areases).

Table S7. Atomic parameters and thermal displacement parameters (Å$^2$) for $Ba_{10}(PO_4)_6(OH_y)_2$*0.05$Co_2O_3$ (sample **4**). $R_{wp}$ = 0.020, $R_{all}$ = 0.019.

| Atom | Ba(1) | Ba(2) | P | O(1) | O(2) | O(3) | O(4) |
|---|---|---|---|---|---|---|---|
| Site | 4f | 6h | 6h | 6h | 6h | 12i | 4e |
| SOF | 1 | 1 | 1 | 1 | 1 | 1 | 0.5 |
| $x$ | 1/3 | 0.2400(2) | 0.4014(8) | 0.3330(18) | 0.5752(18) | 0.3472(11) | 0 |
| $y$ | 2/3 | 0.9820(3) | 0.3681(9) | 0.4807(19) | 0.460(2) | 0.2684(11) | 0 |
| $z$ | -0.0011(5) | 1/4 | 1/4 | 1/4 | 1/4 | 0.0881(12) | 0.111(3) |
| $U_{eq}$, $U_{iso}$ | 0.0135(8) | 0.0150(14) | 0.005(2) | 0.012(6) | 0.010(5) | 0.017(4) | 0.043(13) |
| $U_{11}$ | 0.0140(11) | 0.0132(18) | | | | | |
| $U_{22}$ | 0.0140(11) | 0.0124(17) | | | | | |
| $U_{33}$ | 0.0127(13) | 0.0155(12) | | | | | |
| $U_{12}$ | 0.0070(5) | 0.0035(17) | | | | | |
| $U_{13}$ | 0 | 0 | | | | | |
| $U_{23}$ | 0 | 0 | | | | | |

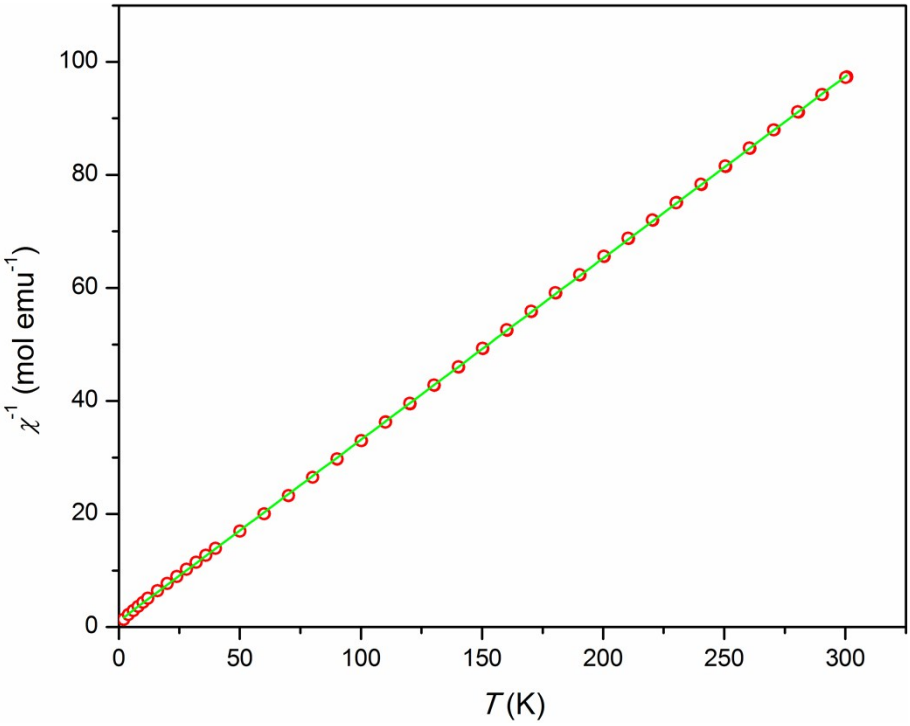


Figure S12. Inverted dc-susceptibility $\chi^{-1}$ per 1 mol of Co vs. temperature $T$ in a field of 5 kOe for **4**. Symbols – experimental points. Line – fitting with eq. $\chi = C/(T - \theta) + \chi_{TIP}$, $C$ = 3.119(8) emu K mol$^{-1}$, $\theta$= -3.2(1) K, $\chi_{TIP}$ = -2(3)*10$^{-5}$ emu mol$^{-1}$, $R^2$ = 0.99997; $\mu_{eff}$ = 4.99(1) $\mu_B$.

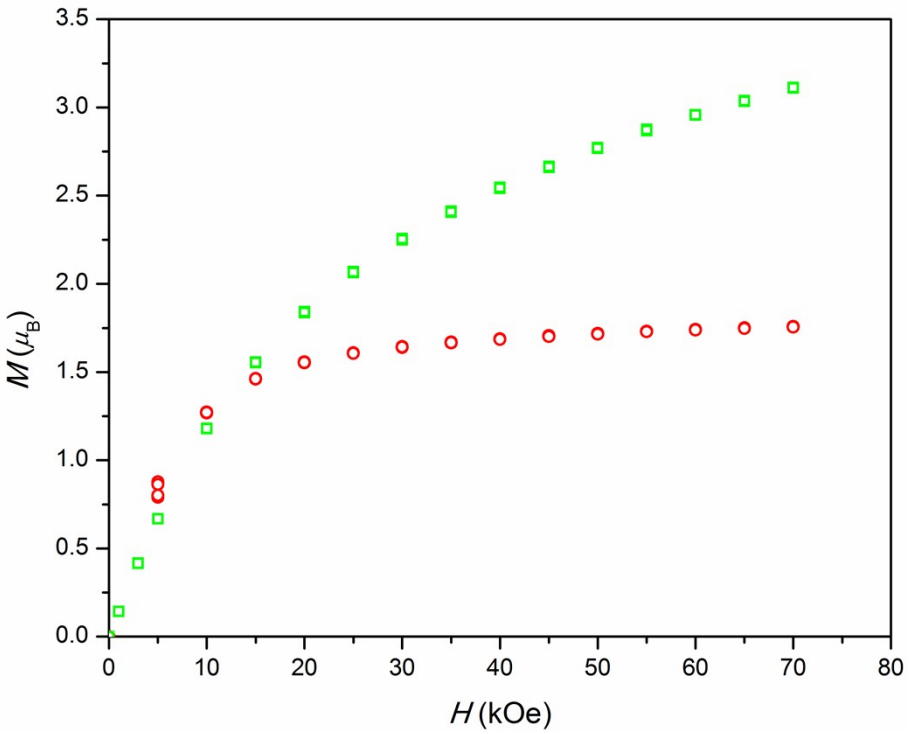


Figure S13. Magnetization (M) per 1 atom of Co vs. magnetic field (H) at 1.8 K. Circles – **2**, Squares – **4**. Measured points are for field up from 0 to 70 kOe and down to 0 kOe. Two points were measured at each field with time interval of 50 s. **4** shows no hysteresis and relaxation. **2** shows hysteresis only at $H$ = 0.5 kOe, the second point for fields both up and down is shifted due to the magnetization relaxation.

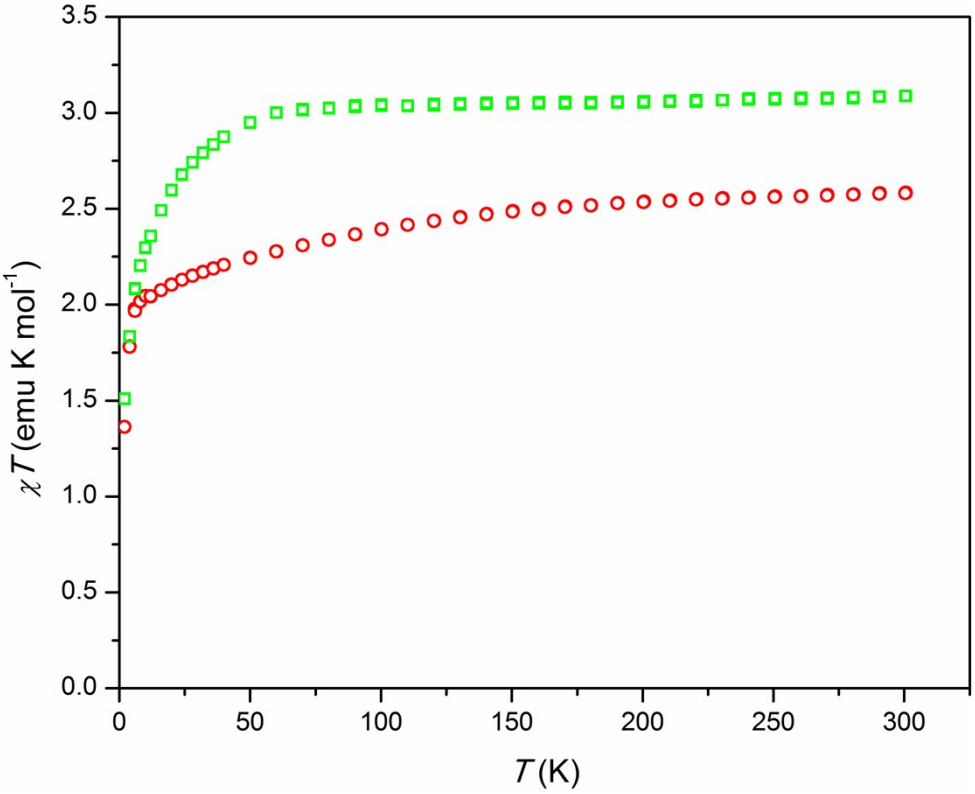


Figure S14. Product $\chi T$ per 1 mol of Co vs. temperature ($T$). Circles – **2**. Squares – **4**.

**Modeling electronic structure and magnetic susceptibility using program CONDON.**

Imput parameters.

7 d-electrons, 120 basis electron states. Racah parameters ($Co^{2+}$), $B$ = 1115 $cm^{-1}$, $C$ = 4366 $cm^{-1}$. Spin-orbital coupling constant $\xi$ = 533 $cm^{-1}$, orbital reduction factor 0.84 (isotropic). Crystal field parameters (Wybourne notation), $B_{20}$ = 24000 $cm^{-1}$, $B_{40}$ = 12000 $cm^{-1}$, $B_{22}$ = 3600 $cm^{-1}$, $B_{42}$ = 1800 $cm^{-1}$, $B_{44}$ = 1700 $cm^{-1}$.

Output parameters.

Table S8. Energies of first 10 energy doublets and their (negative) magnetic moments under a field of 10 kOe for spins antiparallel (upper row) and parallel (lower row) to the magnetic field.

| Energy in zero field ($cm^{-1}$) | $\mu_z$ ($\mu_B$) | $\mu_x$ ($\mu_B$) | $\mu_y$ ($\mu_B$) |
|---|---|---|---|
| 0.0000E+00 | -0.4994E+01 | -0.1606E+00 | -0.1375E+00 |
| | 0.4992E+01 | 0.1392E+00 | 0.1231E+00 |
| 0.3351E+03 | -0.2089E+01 | -0.1804E+01 | -0.1891E+01 |
| | 0.2082E+01 | 0.1820E+01 | 0.1903E+01 |
| 0.1305E+04 | -0.5239E-01 | -0.1480E+01 | -0.2138E+01 |
| | 0.5998E-01 | 0.1463E+01 | 0.2124E+01 |
| 0.1628E+04 | -0.1115E+01 | -0.2453E+00 | -0.2453E+00 |
| | 0.1117E+01 | 0.2635E+00 | 0.2602E+00 |
| 0.2560E+04 | -0.2427E+00 | -0.3589E+00 | -0.3360E+01 |
| | 0.2877E-01 | 0.5953E-01 | 0.3356E+01 |
| 0.2583E+04 | -0.2029E+01 | -0.1756E+01 | -0.1099E+01 |
| | 0.2243E+01 | 0.2054E+01 | 0.1101E+01 |
| 0.5398E+04 | -0.3797E+01 | -0.3705E-01 | -0.3886E-01 |
| | 0.3796E+01 | 0.1297E-01 | 0.1085E-01 |
| 0.5588E+04 | -0.1519E+01 | -0.1703E+01 | -0.1587E+01 |
| | 0.1516E+01 | 0.1719E+01 | 0.1611E+01 |
| 0.5993E+04 | -0.2433E+00 | -0.4388E+00 | -0.2744E+01 |
| | 0.2423E+00 | 0.4269E+00 | 0.2738E+01 |
| 0.6201E+04 | -0.1865E+01 | -0.8761E+00 | -0.8399E+00 |
| | 0.1869E+01 | 0.8986E+00 | 0.8494E+00 |

**Fitting of $\Delta\chi$ (see Fig. 4 insert and the main text).**

Model of a Heisenberg dimer. $\Delta\chi = \frac{FNg^2\mu_B^2}{6k_BT} \cdot \frac{6\exp(2J/k_BT) + 30\exp(6J/k_BT) + 84\exp(12J/k_BT)}{1 + 3\exp(2J/k_BT) + 5\exp(6J/k_BT) + 7\exp(12J/k_BT)} + \chi_{TIP}$.

$F$ = 0.140(3), $g$ = 2 (fixed), $J$ = -25.1(3) $cm^{-1}$, $\chi_{TIP}$ = 0.00021(2) emu $mol^{-1}$, $R^2$ = 0.982. $F$ is a fraction of Co ions left after the exclusion of the FR fraction (90%). Then a fraction of all Co ions present in the sample, which is found in the proposed dimer, is $F$*90% = 13%.

**References**


1 M. Drakopoulos, Th. Connolley, C. Reinhard, R. Atwood, O. Magdysyuk, N. Vo, M. Hart, L. Connor, B. Humphreys, G. Howell, S. Davies, T. Hill, G. Wilkin, U. Pedersen, A. Foster, N. De Maio, M. Basham, F. Yuan, K. Wanelik. I12: the Joint Engineering, Environment and Processing (JEEP) beamline at Diamond Light Source. *J. Synchrotron Rad.* 2015, **22**, 828-838.

2 J. Filik, A.W. Ashton, P.C.Y. Chang, P.A. Chater, S.J. Day, M. Drakopoulos, M. Gerring, M.L. Hart, O.V. Magdysyuk, S. Michalik, A. Smith, C.C. Tang, N. J. Terrill, M.T. Wharmby and H. Wilhelm. Calibration and Processing of Powder-Diffraction Data in DAWN. *J. Appl. Cryst.* 2016 (submitted).

3 M. Basham, J. Filik, M.T. Wharmby, P.C.Y. Chang, B.E. Kassaby, M. Gerring, J. Aishima, K. Levik, B.C.A. Pulford, I. Sikharulidze, D. Sneddon, M. Webber, S.S. Dhesi, F. Maccherozzi, O. Svensson, S. Brockhauser, G, Naray and A.W. Ashton. Data Analysis WorkbeNch (DAWN). *J. Synchrotron Rad.* 2015, **22**, 853–858.

4 V. Petříček, M. Dušek, L. Palatinus. Crystallographic Computing System JANA2006: General Features. *Z. Kristallogr.-Cryst. Mater.* 2014, **229**, 345-352.

5 S. M. J. Aubin, Z. Sun, L. Pardi, J. Krzystek, K. Folting, L.-C. Brunel, A. L. Rheingold, G. Christou and D. N. Hendrickson. Reduced Anionic $Mn_{12}$ Molecules with Half-Integer Ground States as Single-Molecule Magnets. *Inorg. Chem.* 1999, **38**, 5329-5340.